Human cells based directed evolution of adenine base editors with improved efficiency

Junhao Fu
Wenzhou Medical University
Qing Li
State Key Laboratory of Cell Biology, Shanghai Key Laboratory of Molecular Andrology, CAS Center for Excellence in Molecular Cell Science, Shanghai Institute of Biochemistry and Cell Biology
https://orcid.org/0000-0002-6392-9699
Xiaoyu Liu
Wenzhou Medical University
Tianxiang Tu
Affiliated Eye Hospital of Wenzhou Medical University
Xiujuan Lv
Affiliated Eye Hospital of Wenzhou Medical College
Xidi Yin
University of Chinese Academy of Sciences
Zongming Song
Affiliated Eye Hospital of Wenzhou Medical University https://orcid.org/0000-0001-5869-7312
Jinwei Zhang
National Institutes of Health https://orcid.org/0000-0002-2114-173X
Jinsong Li
State Key Laboratory of Cell Biology, Shanghai Institute of Biochemistry and Cell Biology, Center for Excellence in Molecular Cell Science, Chinese Academy of Sciences https://orcid.org/0000-0003-3456-662X
Feng Gu (gufenguw@gmail.com)
Affiliated Eye Hospital of Wenzhou Medical University

Article

Keywords: ABE, Variants, Activity, Directed evolution

Posted Date: May 6th, 2021

DOI: https://doi.org/10.21203/rs.3.rs-418740/v1

Version of Record: A version of this preprint was published at Nature Communications on October 8th, 2021. See the published version at https://doi.org/10.1038/s41467-021-26211-0.

Human cells based directed evolution of adenine base editors with improved efficiency

Junhao Fu[1&], Qing Li[2&], Xiaoyu Liu[1&], Tianxiang Tu[1], Xiujuan Lv[1], Xidi Yin[2], Zongming Song[1,3], Jinwei Zhang[4], Jinsong Li[2*], and Feng Gu[1*]

[1]School of Ophthalmology and Optometry, Eye Hospital, Wenzhou Medical University, State Key Laboratory and Key Laboratory of Vision Science, Ministry of Health and Zhejiang Provincial Key Laboratory of Ophthalmology and Optometry, Wenzhou, Zhejiang, China

[2]State Key Laboratory of Cell Biology, Shanghai Key Laboratory of Molecular Andrology, CAS Center for Excellence in Molecular Cell Science, Shanghai Institute of Biochemistry and Cell Biology, Chinese Academy of Sciences, Shanghai, China.

[3]Henan Eye Hospital, Henan Eye Institute, Henan Provincial People's Hospital and People's Hospital of Zhengzhou University, Zhengzhou, Henan 450052, China.

[4]Laboratory of Molecular Biology, National Institute of Diabetes and Digestive and Kidney Diseases, National Institutes of Health, Bethesda, Maryland, USA.

[&]These authors contributed equally to this work.

* **Correspondence:**

Feng Gu, **E-mail**: gufenguw@gmail.com, Jinsong Li, **E-mail**: jsli@sibcb.ac.cn

Abstract

Adenine base editors (ABE) are novel genome-editing tools that have been harnessed to introduce precise A•T to G•C conversion in genomic DNA. However, the low activity of ABE remains a major bottleneck that precludes efficacious applications. To address this limitation, we developed a directional screening system in human cells to evolve the deaminase component of the ABE, and identified three high-activity NG-ABEmax variants: NG-ABEmax-SGK (R101S/D139G/E140K), NG-ABEmax-R (Q154R) and NG-ABEmax-K (N127K). With further engineering, we created a new, consolidated variant [NG-ABEmax-KR (N127K/Q154R)] which exhibited superior editing activity both in human cells and in mouse disease models, compared to the original NG-ABEmax. We also found that NG-ABEmax-KR efficiently introduce natural mutations in gamma globin gene promoters with more than four-fold increase in editing activity. This work provides a broadly applicable, rapidly deployable platform to directionally screen and evolve novel, user-specified traits in base editors that extend beyond augmented editing activity.

Key words: ABE; Variants; Activity; Directed evolution

Introduction

Recent advances in genome engineering technologies based on CRISPR-Cas9 are enabling the systematic interrogation of mammalian genome functions and numerous targeted medical applications [1-3]. Cas9-triggered double-strand DNA break (DSB) at a target sequence in the genome is subsequently repaired by non-homologous end joining (NHEJ), microhomology-mediated end joining (MMEJ), or homology-directed repair (HDR) [1,4]. CRISPR-Cas9 incurs toxicity because it generates DSBs and off-target mutations that are more prone to occur when a nuclease-induced DSB is present [5]. Base editing is a genome-editing method that directly generates precise point mutations without creating DSBs [7]. As base editors do not produce DSBs, they minimize the off-target effect, compared with CRISPR-Cas9 mediated editing [2].

The current base editing technology can be classified into DNA and RNA base editors. As to the first one, two classes of DNA base editor have been reported: cytosine base editors (CBE) which convert a C•G base pair into a T•A pair, and adenine base editors (ABE) which convert an A•T base pair into a G•C pair [2,3]. CBE and ABE can mediate all four possible transition mutations (C to T, A to G, T to C and G to A). Base editors have been successfully implemented in various organisms including human cells, animals and plants[6-12]. Nevertheless, the gene-editing utility of base editors is hampered by low efficiency and the off-target effect [13,14]. ABE are particularly limited due to its lower efficiency compared with CBE [15].

To overcome these limitations, several strategies have been adopted to increase the activity of ABE. These include optimizing the codon usage of ABE, modifying the location and number of nuclear localization signals (NLS), reconstructing ancestral deaminase component and using different forms of sgRNA [10,16-19]. These extensive efforts reflect an urgent need to optimize ABE as an effective gene-edi ting tool. Additional questions also need to be addressed, including the control of the editing window for improved target site selection. By introducing F148A mutation in both the evolved TadA domain (TadA*) and the wild-type TadA domain (TadA), engineered ABE possessed the higher fidelity without RNAase editing side effect, also its editing window has been narrowed [20]. However, for certain sites, such as when the target base exceeds the canonical editing window relative to the available PAM (protospacer adjacent motif) or the gene is inactivated by introducing premature termination codons, a wider editing window may be more desired. Here,

with directed evolution in human cells, we sought to establish a general screening platform to engineer NG-ABEmax to identify variants with special traits, i.e., enhanced activity.

Results

Generation of a high-throughput *EGFP*-based screening system for adenine base editors

To engineer and augment the existing adenine base editors, we first sought to generate a human cell-based reporter system that allows for rapid and accurate determination of ABE activity and specificity. We previously established an EGFP-reporter system in human cells to evaluate the efficiency of CRISPR-Cas9 and CRISPR-Cas12a [21-27]. Herein, when the sequence-specific RNA-guided endonuclease is targeted to the coding region of *EGFP*, it may generate frameshift indel mutations that lead to loss of fluorescence. However, such a screening system is ineffectual to evaluate ABE mutants, because the editing of one or more adenosines to guanosines at different regions of the *EGFP* sequence leads to diverse local protein alterations that can exhibit highly variable effects on *EGFP* folding, structure, and consequently its fluorescence, thus confounding analysis by cytometry.

To create a screening system where base editing completely ablates, rather than unpredictably alters *EGFP* activity, we first tested if ABE editing of a tryptophan TGG codon in *EGFP* (W58) to an amber stop codon TAG inactivates *EGFP* by truncating the protein near its N-terminus [10] (Supplementary Fig. 1a). We observed that the green fluorescence of *EGFP* was abolished by this conversion, suggesting feasibility of this approach (Supplementary Fig. 1b). To avoid any potentially confounding effects of editing neighboring non-target adenosines that flank the W58 site, we then sought to replace all adjacent adenosines with other nucleobases while maintaining *EGFP* activity (Fig. 1a). While the 13 nucleotides upstream of W58 contained no adenosines, the 18 nucleotides downstream of W58 harbor three adenosines, all part of ACC codons encoding Threonine. By mutating the three ACC codons to TCG, we introduced three conservative substitutions: T60S, T63S and T64S, and found that the mutations do not appreciably impact *EGFP* fluorescence (Fig. 1a-c). Lastly, we created a 5'-TG-3' PAM (protospacer adjacent motif) site necessary for Cas9 recognition through a silent mutation (CTC-to-CTG coding for L61). We term this engineered *EGFP* target gene that harbors all four mutations "*EGFP* variant", which exhibited comparable EGFP expression levels as the wild-type (Fig. 1a-c).

Base editors such as ABE exhibit variable editing efficiencies at different adenosine sites within the editing window [3]. To measure the positional effects on editing efficiency and to identify an

optimal site for subsequent variant screening, we generated 12 partially overlapping single guide RNAs (sgRNAs) that allow the single editing site to shift gradually from the 5' end (position A1), to near the 3' end (position A16) of a 20-nucleotide sliding window. To enable single-nucleotide step scanning in a compact editing window (Fig.1d, e), we used NG-ABEmax to edit either an amber stop codon (TAG, *dEGFP1*) or an opal stop codon (TGA, *dEGFP2*) back to TGG (encoding W58), thus restoring full-length *EGFP* transcription and leading to an increase in fluorescence (Fig.1f, g).

Consistent with previous reports [3], our edit site scan analysis revealed a wide editing efficiency distribution centered around A6 and A7 with efficiencies ranging from 0.05% (A16) to 48% (A6), suggesting both robust editing efficacy and high site selectivity of the assay system (Fig. 1f-g).

Evolution of NG-ABEmax variants with higher editing activity

To demonstrate practical utility of our stop codon reversion-based screening system for adenine base editors, we used it to screen for NG-ABEmax variants that exhibit augmented editing efficiencies. To this end, it is appropriate to select an editing site with low-to-intermediate editing efficiency with the current NG-ABEmax, so that any significant activity enhancement can be captured and accurately quantified. We selected A12 site with a 3.1% efficiency (Fig. 1f), which also falls outside the canonical editing window of NG-ABEmax, to screen for variants with either a generally augmented editing activity, or an ability to edit in a shifted window.

We first generated two random variant libraries of NG-ABEmax by error-prone PCR and named them library 1 and library 2 (Fig. 2a, Supplementary Fig. 2a), which carry mutations in the evolved TadA domain (TadA*) or the wild-type TadA domain (TadA), respectively. Library 1 produced about 1428 colonies (numbered L1-1 to L1-1428), and library 2 had 550 colonies (numbered L2-1 to L2-550). To estimate the frequency of mutagenesis, we randomly picked 20 colonies per library for Sanger sequencing. Sequencing analysis revealed that 19 of the 20 colonies from library 1 harbored unique mutation(s), while the 20th colony had a single-nucleotide deletion. Very similar results (19 colonies with unique mutation(s); one with deletion) were obtained with library 2. Further analysis revealed an average rate of ~4.8 substitutions per kilobase in these two libraries (Supplementary Table 1).

Subsequently, each variant (L1-1 to L1-1428 and L2-1 to L2-550 plasmids) was individually co-transfected with the corresponding sgRNA (*dEGFP1*-A12) and *dEGFP1* expression cassette into HEK-293 cells (Supplementary Fig. 2b), respectively. We found that 12 (8 of library 1 and 4 of library 2) out of the 1978 tested variants exhibited significantly elevated activity at A12, showing at

least a 3-fold increase in editing activity (8.9%-11.25%), compared to the wild-type NG-ABEmax (2.62%-3.4%) (Fig. 2b). These findings suggest that the screening platform is effective at identifying and enriching high-activity base editor variants.

To distinguish whether these 12 high-activity variants possess generally higher activity at all target sites or shift or expand the editing window to gain activity at the A12 site, we took advantage of our recently developed method for assessing base editing in human cells, in which editing efficiency is measured by agarose-gel analysis of editing-mediated inactivation of restriction enzyme sites [15]. We generated a sgRNA that can simultaneously target a PstI restriction site (A7) and a SalI restriction site (A12) in the MCS (multiple cloning sites) sequence, which was integrated into the genome of HEK-293 (termed HEK293-PME) (Fig. 2c). Each of these 12 variants was then co-transfected with this sgRNA into HEK293-PME cells. At 48 h post-transfection, cells were collected and isolated genomic DNA. PCR was performed with the genomic DNA as a template with specific primers. Purified PCR products were treated with PstI (178 bp + 428 bp) or SalI (177 bp + 429 bp), respectively, and then analyzed by agarose gel electrophoresis to estimate editing efficiency. Remarkably, L1-60, L1-98 and L2-156 showed significantly improved activity (more than ~3-fold increase) at A7 site (Fig. 2d). While, it may be due to the low sensitivity of this restriction enzyme digestion-based method, we can't observe the boosting effects at A12 site, (Supplementary Fig. 3). The enhanced editing efficiencies of L1-60, L1-98 and L2-156 were further confirmed with above-described *EGFP*-based flow cytometry system (Fig. 2e). Notably, L2-156 possesses the highest activity among all tested variants, with ~2-fold increase in editing efficiencies at A7 and A9 sites. These results suggest that these three variants possessed across-the-board higher editing activities both within and outside of the canonical editing window, rather than merely shifting the editing window.

Mapping the key residues underlying enhanced editing activity

To map the exact sequence changes in L1-60, L1-98 and L2-156, we sequenced the TadA* domains of L1-60 and L1-98 and the TadA domain of L2-156. We found multiple amino acid substitutions in L1-60 (R101S/D139G/E140K), L1-98 (E9K/Q154R), and L2-156 (A106S/N127K/E155K), respectively. To deconvolute any combinatory effects and identify key residues that drove higher editing activities in L1-60, L1-98 and L2-156, we dissected all possible single, double, and triple combinations of mutations found in these 3 variants using our *EGFP*-based system (Fig. 3a and Supplementary Fig. 4).

For L1-60, the highest activity occurred when R101S, D139G and E140K were present simultaneously (hereafter termed NG-ABEmax-SGK, Fig. 3a). For L1-98, the performance of Q154R alone was comparable to that of E9K/Q154R. Therefore, Q154R is the key mutation for the enhanced activity of L1-98, and the variant harboring singe Q154R mutation termed NG-ABEmax-R (Fig. 3a). For L2-156, N127K alone accounted for essentially all the enhanced activity. The activity enhancement was completely abolished when N127K was reverted back to WT. Thus, N127K substitution was the driving force for the enhanced activity in L2-156 and is hereafter referred to as NG-ABEmax-K (Fig. 3a). Meanwhile, NG-ABEmax-R and NG-ABEmax-K have slightly higher activity, compared with that of NG-ABEmax-SGK (Fig. 3a).

As these high-efficiency variants were identified and validated on an exogenous *EGFP* gene, we next verified that they also function similarly at endogenous genomic loci. To this end, we transfected HEK-293 cells with these two variants NG-ABEmax-R or NG-ABEmax-K to edit a panel of 19 genomic sites of different sequence context and composition. Upon editing, genomic DNA was extracted from harvested cells at 48 h post-transfection and next-generation sequencing was performed.

Compared to NG-ABEmax, NG-ABEmax-SGK, NG-ABEmax-R and NG-ABEmax-K exhibited significantly improved editing efficiency at most genomic sites tested ((Supplementary Fig. 5,6). The enhancement was particularly pronounced at low-efficiency sites. For NG-ABEmax-R, the enhanced activity was most obvious at A4 (average: 14.62% of NG-ABEmax-R versus 2.94% of NG-ABEmax), an increase of 5.0-fold (Supplementary Fig. 5, 6b). For NG-ABEmax-K, the average activity increased by 2.2-fold at A7 where the enhanced activity was most evident compared to NG-ABEmax (average: 28.96% of NG-ABEmax-K versus 13.04% of NG-ABEmax) (Fig. 3b, Supplementary Fig. 6c). Mirroring the findings on the *EGFP* gene, the editing activity of these variants on genomic sites had been significantly improved both within and outside of the canonical editing window (Fig. 3, Supplementary Fig. 6). Notably, at the non-canonical editing window (i.e., A12), the activity of these variants remains very low, despite significant enhancement by the mutations (Fig. 3a). We also noticed that the editing activity of NG-ABEmax-K was highest among these variants at the majority of sites we examined (Fig. 3a. Supplementary Fig. 6). Taken together, we identified the key editing-enhancing residues of L1-60 (R101S/D139G/E140K), L1-98 (Q154R) and L2-156 (N127K), and showed that these substitutions led to general enhancement of editing activity at both exogenous and endogenous sites and both within and outside the canonical editing window.

Combinatorial optimization of high-efficiency NG-ABEmax variants

NG-ABEmax-K was selected for further study due to its highest editing activity. We hypothesized that replacing Asn127 in TadA with two other basic amino acids [Histidine (H) or Arginine (R)] may produce a similar effect due to similar charge. We generated NG-ABEmaxH^{127} and NG-ABEmaxR^{127} and tested the performance (Supplementary Fig. 5). Interestingly, we found that while N127H had little effect on activity, N127R exhibited enhanced activity comparable to N127K within the canonical editing window (Supplementary Fig. 7a). This was most obvious at A7 (ranging from 2.73% to 64.98%, compared to NG-ABEmax [ranging from 1.3% to 48.1%)], with up to 6.02-fold increase on site 3 (Supplementary Fig. 7b). These data suggest that a long-chain basic residue at position 127 in TadA generally boosts the editing efficiency of NG-ABEmax, potentially by enhancing local interactions with the DNA substrate.

We next sought to further enhance the activity by combining mutations from NG-ABEmax-R, and NG-ABEmax-K, because using our EGFP-based system these two have slightly higher activity, compared with that of NG-ABEmax-SGK (L1-60, Fig. 3a). We generated a variant namely NG-ABEmax-KR (N127K mutation in TadA domain, Q154R mutation in TadA* domain) (Supplementary Fig. 5). We evaluated the activity at the endogenous genomic sites and found that NG-ABEmax-KR exhibited further increased activity (Fig. 3b, Supplementary Fig. 8). Specifically, the average activity of NG-ABEmax-KR was increased by 1.1-fold to 5.4-fold within the canonical editing window, with an activity ranging from 40.87% to 64.22% (7.6% to 60.27% for NG-ABEmax) (Supplementary Fig. 8). Upon additional examination, we found that the editing window has been greatly expanded in both directions in NG-ABEmax-KR (Fig. 3c-e, Supplementary Fig. 9). Specifically, compared with canonical editing window at the A4~A7, the NG-ABEmax-KR has an editing window at A3~A7, with a substantially higher activity at A3, A4, A6 and A7. These finding show that the original mutations acted partially or wholly independently of each other, thus allowing further enhancements by combinatorial optimization.

NG-ABEmax-KR exhibits superior efficacy in mice disease models and human gene therapy

To test whether NG-ABEmax-KR could be harnessed for efficient generation of mouse disease models, we designed an sgRNA to target c.202 of *Tyr* gene encoding the melanin-producing Tyrosinase, to introduce a missense codon (CAT to CGT, H420R) and generate an albinism mouse model[28] (Fig. 4a). Successful editing would produce *Tyr* mutant mice that have white skin instead of wild-type mice with black skin (Fig. 4b). Remarkably, the efficiency of base editing in the mouse

model by NG-ABEmax-KR was drastically higher than the original NG-ABEmax (Fig. 4c). While the original NG-ABEmax produced only 1 (9%) white and 2 (18%) mosaic (white/black) mice out of 11 in total, the NG-ABEmax-KR produced 15 (75%) white and 2 (10%) mosaic mice out of 20 in total. Next-generation sequencing of the target site from each mouse showed that the editing efficiency were greatly boosted at A3 (Fig. 4c, Supplementary Fig. 10), consistent with the phenotype results. Sanger sequencing further confirmed the successful editing events at the target site (Fig. 4d).

Next, we sought to evaluate the performance of NG-ABEmax-KR in introducing disease-correcting mutations. An effective therapeutic strategy that greatly alleviate the clinical symptoms of β-globin diseases such as sickle-cell anemia and β thalassaemia is to recapitulate British-type HPFH and induce fetal hemoglobin production in adults by promoter manipulation [29]. To this end, we designed a sgRNA to simultaneously mutate the *HBG1* or *HBG2* (*HBG1/HBG2*) *p*romoters to activate their expression. We found that in HEK-293 cells, NG-ABEmax-KR efficiently installed the desired T•A to C•G mutations in *HBG1/HBG2* promoters, with a 4.32-fold increase in editing efficiency over NG-ABEmax (Fig. 4e).

Enhanced gene-editing activity is generally associated with an elevated off-target activity. To ask whether NG-ABEmax-KR increases off-target effects, we amplified fragments harboring the target site by PCR and performed sequencing to detect potential off-target editing. We observed a slight increase in editing at three off-target sites compared to NG-ABEmax (Supplementary Fig.11). We also investigated the off-target effects of targeting *Tyr* gene for generation of mice disease models by the prediction of potential off-target sites, and observed no off-target at the majority of the predicted sites (Supplementary Fig.12). We did observe off-target editing at certain other sites. These findings are consistent with the notion that NG-ABEmax-KR enhances the general catalytic activity of TadA that are manifest at both target and non-target sites. To address whether NG-ABEmax-KR could increase the on-target:off-target editing ratios, we performed the analysis of on-target and its off-target. The results revealed a dramatic increase of NG-ABEmax-KR (up to 4037-fold at *HEK 3*-A6-OT4 of NG-ABEmax-KR VS 1432-fold of NG-ABEmax) at the off-target sites analyzed except one (*HEK 2*-A7-OT2, Supplementary Fig.13). Together, these applications in mouse disease models and human gene therapy show that NG-ABEmax-KR is an effective gene-editing tool that exhibits superior activity in both human cells and animal models.

Molecular underpinnings of the enhanced editing efficiency of NG-ABEmax-KR

To gain a mechanistic understanding of NG-ABEmax-KR's enhanced editing efficiency, we performed structural modeling. Structural modeling suggests that substitutions of the DNA-facing

side chains of N127 of TadA* and Q154 of TadA with longer, positively charged side chains may create new, stabilizing interactions with the editing window, potentially augmenting catalysis (Fig.5a, b). Specifically, an N127K substitution is expected to bring its e-ammonium group within hydrogen-bonding distance (~3.6 Å) with the backbone non-bridging oxygen (OP1) of C27, immediately 3′ of the deamination site. This notion is consistent with our observation that N127R had a comparable impact on editing activity as N127K while N127H did not. On the opposite side of the DNA substrate, a Q154R substitution of TadA is projected to insert its guanidinium group between the nucleobases of C24 and C25, two nucleosides that immediately precede the deamination site (A26) on the 5′ side. Here, the Q154R guanidinium group would be located less than 3.5 Å away from both nucleobases of C24 and C25, and well positioned to make robust cation-p interactions to both, thereby stabilizing the DNA conformation to facilitate catalysis. Thus, *in silico* mutagenesis and structural modeling provide a straightforward explanation for the enhanced activity of NG-ABEmax-KR. Further, our findings provide a proof-of-principle that structure-informed rational redesign of the TadA-DNA interface, in particular, by introducing long, basic side chains at strategical locations, can effectively repurpose an enzyme interface originally evolved to recognize RNA hairpins, to recognize and accommodate topologically constrained, single-stranded DNA substrates.

Discussion

ABE are particularly promising tools for the studies and applications of gene therapy, because two-thirds of human diseases are caused by single nucleotide mutations, and about half of these can be corrected by A-to-G conversions [30]. However, ABE currently have limited applications due to low editing activity compared with CBEs. Due to the lack of a clear understanding of the artificial TadA-DNA interface within ABE, rational design-based activity optimizations have not borne significant fruit. In this study, we established and applied an *EGFP*-based screening system to efficiently evolve and select NG-ABEmax variants with desired traits, such as those with increased activity. Using this system, we obtained several mutants (NG-ABEmax-SGK, NG-ABEmax-R, and NG-ABEmax-K) that possess higher editing activity (Figs. 2-4). Besides higher editing efficiency, these three variants are able to effectively editing at certain inaccessible positions by the wild-type NG-ABEmax (Fig. 2). Among the three variants NG-ABEmax-K exhibited the best performance at most sites we examined (Fig. 3b, Supplementary Figs. 5-6). To further enhance the activity, NG-ABEmax-KR was created by the combinatorial design using the identified driver mutations (Fig.

3b, c, Supplementary Fig. 8). Compared with NG-ABEmax, NG-ABEmax-KR showed superior editing activity and an expanded editing window (Fig. 3, 4).

The Cas9 element in ABE has been extensively studied as a limiting factor for PAM recognition [31-37]. However, some studies have illustrated that Cas9 elements are also responsible for the editing window of ABE, which indicates that the Cas9 element may also be selected for the evolution of ABE [31,33,38,39]. In addition, the sequence or structure of the sgRNA may also modulate the activity of ABE, suggesting it could be further optimized [10]. As for DNA off-target effects, we characterized the fidelity of NG-ABEmax and its variants (Supplementary Fig. 11, 12, 13). It is reported that ABE can also induce RNA off-target effects contributed by the wild-type TadA domain [20,40-42]. If we deleted the wild-type TadA domain, RNA off-target effects may be ameliorated. In addition to editing canonical base A by ABE, multiple studies have found that ABE can also edit base C at a low level [12,40,43,44]. Nonetheless, our study did not observe off-target editing products involving base C editing. The precise specificity of the NG-ABEmax variants awaits further comprehensive characterization.

While our study was being prepared for publication, Richter and colleagues reported directed evolution of ABEmax based on phage-assisted non-continuous and continuous evolution (PANCE and PACE), which produced ABE8e [45]. Based on the synthetic library of TadA sequences that contains all 20 canonical amino acid substitutions at each position of TadA, Nicole and colleagues identified ABEmax variants (ABE8s) with higher activity [46]. Notably, we observed that the Q154R mutation that we selected was also identified in ABE8s but not ABE8e, suggesting that directional evolution analyses based on different strategies may converge on the same critical sites. Our high-activity mutations do not overlap with those reported in the ABE8e [45,46]. A comparative analysis of the editing efficiencies of ABE8e, ABE8s and NG-ABEmax-KR may yield additional insights into the path leading to improved efficiency and combination of these mutations in the same enzyme may achieve synergistic effects as we observed in this study. Recently, the structure of ABE8e has been reported, which provides additional insights for further rational design of ABE [47].

Taken together, in the present study, we created a high-throughput directional screening system to evolve, select and assess ABE activity in human cells, and identified NG-ABEmax variants with significantly increased editing activity. This system can be readily applied to evolve additional ABE traits besides enhanced activity, such as access to previously inaccessible editing sites, or modulation of off-target effects. Finally, our analysis provides a mechanistic rationale for

the observed activity enhancement, which can guide further optimizations of the TadA-DNA interface.

Material and methods

Plasmid construction

The original plasmid NG-ABEmax expressing the TadA-TadA*-nSpCas9-NG fusion protein was obtained from Addgene (Addgene plasmid #124163). The plasmid pSIN-EGFP containing an *EGFP* gene, *IRES* and *Puromycin* genes were generated as previously described [21]. The sgRNA expression cassettes were generated by standard protocol. Desired point mutations were introduced into the coding sequence of *EGFP* by PCR to generate *EGFP*-variant, *dEGFP1*, and *dEGFP2*. All plasmids were confirmed by Sanger sequencing. The oligonucleotide sequences used for plasmid construction in this study are listed in Supplementary Tables 2-7.

Construction of NG-ABEmax mutant libraries

NG-ABEmax libraries were generated using the protocols which described previously[48]. For the library 1, the NG-ABEmax plasmids were digested with BseRI, and the digested products (backbone) was subsequently purified (8277 bp). Then, GeneMorph II Random Mutagenesis Kit (Agilent) was used to perform error-prone PCR on the TadA* domain in the NG-ABEmax plasmid sequence, and the PCR products were purified as fragments (575 bp). The backbone and fragments were In-fusion assembled (Supplementary Fig 3a). For the library 2, the backbone plasmids were digested with SacII and BamHI (the final products of 8177 bp). Then, fragments (730 bp) of error-prone PCR on the TadA domain were obtained using the same method (Supplementary Fig 3a). The resulting library 1 and library 2 were transformed into electrocompetent *E. coli* DH10B and incubated on LB plates with Ampicillin (0.1 g/mL) at 37℃ overnight. A total of 1978 colonies (1428 of library 1 and 550 of library 2) were obtained. The plasmids from individual colonies were isolated. The oligonucleotide sequences used for libraries construction are listed in Supplementary Table 8.

Cells and cell culture

HEK-293 cells were obtained from ATCC (CAT#CRL-1573), and HEK293-PME cells were generated as previously described [21]. HEK-293 cells were grown at 37℃ in 5% CO_2 in Dulbecco's modified Eagle's medium (Life Technologies, Carlsbad, CA) supplemented with 10% heat-inactivated fetal bovine serum, penicillin/streptomycin. HEK293-PME cells were cultured with additional puromycin [21].

Transfection protocol, genomic DNA extraction, images and flow cytometry analysis

For NG-ABEmax variants screening experiments, HEK-293 cells were seeded at 0.9×10^5 cells per well on 24-well plates in DMEM medium. 24 h after seeding, cells were co-transfected with 200 ng NG-ABEmax variant plasmids, 100 ng sgRNA expression plasmids, 200 ng dEGFP1 plasmids and 1.5 ul TurboFect Transfection Reagent (Thermo Fisher Scientific). Medium was changed at 24 h post-transfection and flow cytometry analysis was performed at 48 h post-transfection. For experiments using HEK293-PME to compare the activity of NG-ABEmax variants, HEK293-PME cells were seeded at 0.7×10^5 cells per well on 24-well plates in the presence of puromycin. 24 h after seeding, cells were co-transfected with 200 ng NG-ABEmax variant, 100 ng sgRNA expression plasmids and 1.5 ul TurboFect Transfection Reagent. Genomic DNA extraction of cells is subsequently performed using genome extraction kit (Vazyme). Images were obtained at 24 h and 48 h post-transfection, and cells were collected at 48 h post-transfection. Flow cytometry analysis was performed with FACSAria II (BD Biosciences).

Comparison of the activity of NG-ABEmax variants using HEK293-PME cells

The genomic DNA was used as template for PCR amplification using corresponding primers and PCR products were subsequently purified and recovered (606 bp). 200 ng purified PCR products were treated with PstI (178 bp + 428 bp) or SalI (177 bp + 429 bp). Finally, the activity of NG-ABEmax variants was determined by agarose gel electrophoresis.

Sanger sequencing for pJET colonies

Sequence flanking the CRISPR target sites for *Try* was PCR amplified, and products were inserted into the vector pJET1.2 (CloneJET PCR Cloning Kit, Thermo Fisher Scientific). The ligated products were transformed into *E. coli*. The corresponding plasmids were isolated and sequenced on an ABI PRISM 3730 DNA Sequencer.

Mice

All animal procedures were carried out in accordance with the current guidelines of the Institutional Animal Care and Use Committee (IACUC) at the Center for Excellence in Molecular Cell Science, Shanghai Institute of Biochemistry and Cell Biology, Shanghai, China. B6D2F1 (C57BL/6×DBA2) female mice were used as oocyte donors. The males (C57BL/6) were used to mate with B6D2F1 females to obtain zygotes. ICR females were used as pseudo-pregnant foster mothers.

In vitro transcription

The mRNA transcriptional templates of NG-ABEmax and NG-ABEmax-KR were amplified by PCR using Phanta Max Super-Fidelity DNA Polymerase (Vazyme), purified by the Universal DNA Purification Kit (TIANGEN) and then transcribed using the mMACHINE T7 ULTRA transcription Kit (Invitrogen) following the manufacturer's instruction. The transcriptional template of *Tyr* sgRNA was amplified from Px330-mCherry plasmids [49](Addgene#98750) and transcribed in vitro using the MEGAshortscript T7 kit (Invitrogen) following the manufacturer's instructions. mRNA and sgRNA were subsequently purified with the MEGAclear Transcription Clean-Up Kit (Invitrogen), resuspended in RNase-free water and then stored at −80 °C.

Microinjection and embryo transfer

The mixture of ABE mRNA (100 ng/μl) and sgRNA (100 ng/μl) was diluted in RNAase-free water, centrifuging at 4°C, 13,400 g for 10 min and then injected into the cytoplasm of zygotes harvested from B6D2F1 females (mated with C57BL/6 males) using a micromanipulator (Olympus) and a FemtoJet microinjector (Eppendorf). The injected embryos were cultured in EmbryoMax KSOM Medium (Sigma-Aldrich) until the two-cell stage and then transferred into oviducts of recipients at 0.5 days post-coitum (dpc). Recipient mothers delivered pups at 19.5 dpc and we analyzed phenotypes of offspring at day 10 after birth.

Next-generation sequencing (NGS)

Extracted genomic DNA from transfected cells or mice tails were performed by standard protocol. NGS library was constructed using genomic DNA as template through two rounds of PCR. First-step PCR amplification of 100-220 bp sequences from on/off-target sites were performed using specific primers. For the second-step PCR amplification, we fixed the barcodes, index and adaptor sequences to the first-step PCR amplification products. The second-step PCR amplification products were purified and pooled, and subsequently subjected to paired-end read sequencing using the Hiseq-PE150 strategy at Novogene (Nanjing, China). Finally, open-sourced "CRISPResso" software (version 1.0.10) was used to analyze the status of base editing. The oligonucleotide sequences used for NGS are listed in Supplementary Tables 9, 10.

Molecular modeling

Single amino-acid substitutions are generated *in silico* using Coot [50]. Side chain orientations are then geometrically optimized in Coot. Molecular graphics are prepared using MacPyMOL (Schrödinger, Inc).

Statistics

All data were expressed as mean ± SD Differences were determined by 2-tailed Student's t-test or Mann-Whitney test between two groups. The criterion for statistical significance was *P < 0.05, **P <0.01, ***P < 0.001, ****P < 0.0001.

Acknowledgments

We thank our group member for technical assistance. This work was supported by grants from National Natural Science Foundation of China (81201181), National Key R&D Program of China [2018YFA0107304], Science Technology project of Zhejiang Province (2017C37176), and Project of State Key Laboratory of Ophthalmology, Optometry and Visual Science, Wenzhou Medical University (J02-20190201), Shanghai Super Postdoctoral Incentive Program, China National Postdoctoral Program for Innovative Talents (BX20200348) and by the Intramural Research Program of the NIH, The National Institute of Diabetes and Digestive and Kidney Diseases (NIDDK) (ZIADK075136).

Conflict of interest

The authors declare that they have a patent (pending) for the screening platform and the mutants in this study.

Data availability

The data that support the findings of this study are available in the Supplementary Materials. The deep sequencing data are available at the NCBI Sequence Read Archive (SRA) (https://www.ncbi.nlm.nih.gov/sra/) under BioProject PRJNA 714183 (SRA: SRR13950186-SRR 13950197; SRR13948600-SRR13948607; SRR13950619-SRR13950626; SRR13958607-SRR13958611; sample accession number, SAMN 18291703); BioProject PRJNA 713866 (SRA: SRR13945386- SRR13945395; sample accession number, SAMN 18273806). Pre-processed data is available upon request.

Author contributions

F.G and J.L designed research, J.F, Q. L, X.L, T.T, X.L and X.Y performed research, J.F, Z.S, J.Z, J.L and F.G. performed data analyses, and J.Z, Q.L, and F.G. wrote the manuscript. All authors have read and approved the final manuscript.

References

1. Hsu, P.D. et al. Development and applications of CRISPR-Cas9 for genome engineering. *Cell* **157**, 1262-1278 (2014).
2. Komor, A.C. Programmable editing of a target base in genomic DNA without double-stranded DNA cleavage. *Nature* **533**, 420-4 (2016).
3. Gaudelli, N.M. et al. Programmable base editing of A*T to G*C in genomic DNA without DNA cleavage. *Nature* **551**, 464-471 (2017).
4. Iyer, S. et al. Precise therapeutic gene correction by a simple nuclease-induced double-stranded break. *Nature* **568**, 561-565 (2019).
5. Hsu, P.D. et al. DNA targeting specificity of RNA-guided Cas9 nucleases. *Nat Biotechnol* **31**, 827-32 (2013).
6. Hess, G.T. et al. Methods and Applications of CRISPR-Mediated Base Editing in Eukaryotic Genomes. *Mol Cell* **68**, 26-43 (2017).
7. Li, G. et al. Highly efficient and precise base editing in discarded human tripronuclear embryos. *Protein Cell* **8**, 776-779 (2017).
8. Ryu, S.M. et al. Adenine base editing in mouse embryos and an adult mouse model of Duchenne muscular dystrophy. *Nat Biotechnol* **36**, 536-539 (2018).
9. Villiger, L. et al. Treatment of a metabolic liver disease by in vivo genome base editing in adult mice. *Nat Med* **24**, 1519-1525 (2018).
10. Li, C. et al. Expanded base editing in rice and wheat using a Cas9-adenosine deaminase fusion. *Genome Biol* **19**, 59 (2018).
11. Kang, B.C. et al. Precision genome engineering through adenine base editing in plants. *Nat Plants* **4**, 427-431 (2018).
12. Liu, Z. et al. Efficient generation of mouse models of human diseases via ABE- and BE-mediated base editing. *Nat Commun* **9**, 2338 (2018).
13. Jin, S. et al. Cytosine, but not adenine, base editors induce genome-wide off-target mutations in rice. *Science* **364**, 292-295 (2019).
14. Zuo, E. et al. Cytosine base editor generates substantial off-target single-nucleotide variants in mouse embryos. *Science* **364**, 289-292 (2019).
15. Lv, X. et al. Development of a Simple and Quick Method to Assess Base Editing in Human Cells. *Mol Ther Nucleic Acids* **20**, 580-588 (2020).

16. Koblan, L.W. et al. Improving cytidine and adenine base editors by expression optimization and ancestral reconstruction. *Nat Biotechnol* **36**, 843-846 (2018).
17. Qin, W. et al. Precise A*T to G*C base editing in the zebrafish genome. *BMC Biol* **16**, 139 (2018).
18. Wang, M. et al. Optimizing base editors for improved efficiency and expanded editing scope in rice. *Plant Biotechnol J* **17**, 1697-1699 (2019).
19. Hua, K. et al. Simplified adenine base editors improve adenine base editing efficiency in rice. *Plant Biotechnol J* **18**, 770-778 (2020).
20. Zhou, C. et al. Off-target RNA mutation induced by DNA base editing and its elimination by mutagenesis. *Nature* **571**, 275-278 (2019).
21. Zhang, Y. et al. Comparison of non-canonical PAMs for CRISPR/Cas9-mediated DNA cleavage in human cells. *Sci Rep* **4**, 5405 (2014).
22. Tu, M. et al. A 'new lease of life': FnCpf1 possesses DNA cleavage activity for genome editing in human cells. *Nucleic Acids Res* **45**, 11295-11304 (2017).
23. Sun, H. et al. A Single Multiplex crRNA Array for FnCpf1-Mediated Human Genome Editing. *Mol Ther* **26**, 2070-2076 (2018).
24. Lin, L. et al. Engineering the Direct Repeat Sequence of crRNA for Optimization of FnCpf1-Mediated Genome Editing in Human Cells. *Mol Ther* **26**, 2650-2657 (2018).
25. He, X. et al. Boosting activity of high-fidelity CRISPR/Cas9 variants using a tRNA(Gln)-processing system in human cells. *J Biol Chem* **294**, 9308-9315 (2019).
26. Xie, H. et al. High-fidelity SaCas9 identified by directional screening in human cells. *PLoS Biol* **18**, e3000747 (2020).
27. Liu, X. et al. Lb2Cas12a and its engineered variants mediate genome editing in human cells. *FASEB J* **35**, e21270 (2021).
28. Kwon, B.S. et al. Molecular basis of mouse Himalayan mutation. *Biochem Biophys Res Commun* **161**, 252-60 (1989).
29. Frangoul, H. et al. CRISPR-Cas9 Gene Editing for Sickle Cell Disease and β-Thalassemia. *N Engl J Med* **384**, 252-260 (2021).
30. Landrum, M.J. et al. ClinVar: public archive of interpretations of clinically relevant variants. *Nucleic Acids Res* **44**, D862-8 (2016).
31. Hua, K. et al. Precise A.T to G.C Base Editing in the Rice Genome. *Mol Plant* **11**, 627-630 (2018).

32. Yang, L. et al. Increasing targeting scope of adenosine base editors in mouse and rat embryos through fusion of TadA deaminase with Cas9 variants. *Protein Cell* **9**, 814-819 (2018).
33. Huang, T.P. et al. Author Correction: Circularly permuted and PAM-modified Cas9 variants broaden the targeting scope of base editors. *Nat Biotechnol* **37**, 820 (2019).
34. Qin, R. et al. Developing a highly efficient and wildly adaptive CRISPR-SaCas9 toolset for plant genome editing. *Plant Biotechnol J* **17**, 706-708 (2019).
35. Ren, B. et al. Cas9-NG Greatly Expands the Targeting Scope of the Genome-Editing Toolkit by Recognizing NG and Other Atypical PAMs in Rice. *Mol Plant* **12**, 1015-1026 (2019).
36. Huang, S. et al. Developing ABEmax-NG with Precise Targeting and Expanded Editing Scope to Model Pathogenic Splice Site Mutations In Vivo. *iScience* **15**, 640-648 (2019).
37. Walton, R.T. et al. Unconstrained genome targeting with near-PAMless engineered CRISPR-Cas9 variants. *Science* **368**, 290-296 (2020).
38. Yang, L. et al. Correction to: Increasing targeting scope of adenosine base editors in mouse and rat embryos through fusion of TadA deaminase with Cas9 variants. *Protein Cell* **10**, 700 (2019).
39. Nguyen Tran, M.T. et al. Engineering domain-inlaid SaCas9 adenine base editors with reduced RNA off-targets and increased on-target DNA editing. *Nat Commun* **11**, 4871 (2020).
40. Grunewald, J. et al. CRISPR DNA base editors with reduced RNA off-target and self-editing activities. *Nat Biotechnol* **37**, 1041-1048 (2019).
41. Grunewald, J. et al. Transcriptome-wide off-target RNA editing induced by CRISPR-guided DNA base editors. *Nature* **569**, 433-437 (2019).
42. Rees, H.A. et al. Analysis and minimization of cellular RNA editing by DNA adenine base editors. *Sci Adv* **5**, eaax5717 (2019).
43. Lee, H.K. et al. Targeting fidelity of adenine and cytosine base editors in mouse embryos. *Nat Commun* **9**, 4804 (2018).
44. Kim, H.S. et al. Adenine base editors catalyze cytosine conversions in human cells. *Nat Biotechnol* **37**, 1145-1148 (2019).
45. Richter, M.F. et al. Phage-assisted evolution of an adenine base editor with improved Cas domain compatibility and activity. *Nature Biotechnology* **38**, 883-891 (2020).

46. Gaudelli, N.M. et al. Directed evolution of adenine base editors with increased activity and therapeutic application. *Nat Biotechnol* **38**, 892-900 (2020).
47. Lapinaite, A. et al. DNA capture by a CRISPR-Cas9-guided adenine base editor. *Science* **369**, 566-571 (2020).
48. Liu, X. et al. Engineered FnCas12a with enhanced activity through directional evolution in human cells. *J Biol Chem*, 100394 (2021).
49. Wu, Y. et al. Correction of a genetic disease in mouse via use of CRISPR-Cas9. *Cell Stem Cell* **13**, 659-62 (2013).
50. Emsley, P. et al. Features and development of Coot. *Acta Crystallogr D Biol Crystallogr* **66**, 486-501 (2010).

Figures

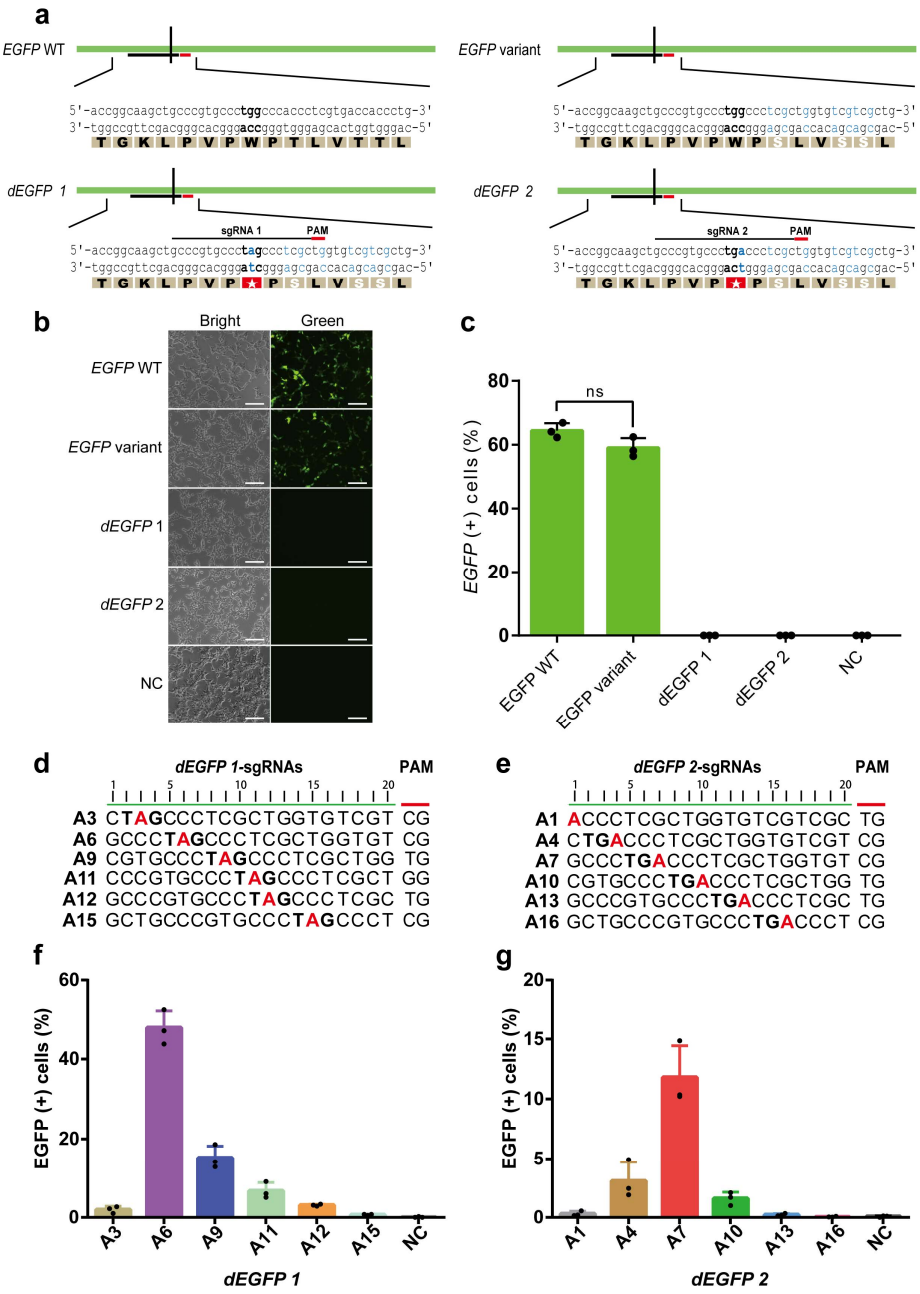

Fig. 1 Design of the stop-codon reversion-based screening system.

a, Different *EGFP* variants. Single nucleotide conversions are indicated by blue and residue substitutions are indicated by white. The stop codon was highlighted with red pentagram. **b, c,** Fluorescence image(**b**) and editing efficiencies(**c**) of HEK-293 cells co-transfect with *EGFP* WT, variant, *dEGFP* 1 and *dEGFP* 2, respectively. *EGFP* variant maintains the expression, while *dEGFP 1* and *dEGFP 2* abolishes the expression. (**c**). EGFP positive cells were quantified by flow cytometry. Scale bar, 10 μm. Data are mean ± s.d. of three technical replicates. **d, e,** The sequence of different sgRNAs (5-'NG-3' PAM) which were suitable for *dEGFP* 1 and *dEGFP* 2, respectively. The stop codon and target A base have been highlighted in bold and red. **f, g,** Editing efficiencies of A to G mutations at different positions of *dEGFP* 1 and *dEGFP* 2. Error bars indicate mean ± s.d. of three technical replicates.

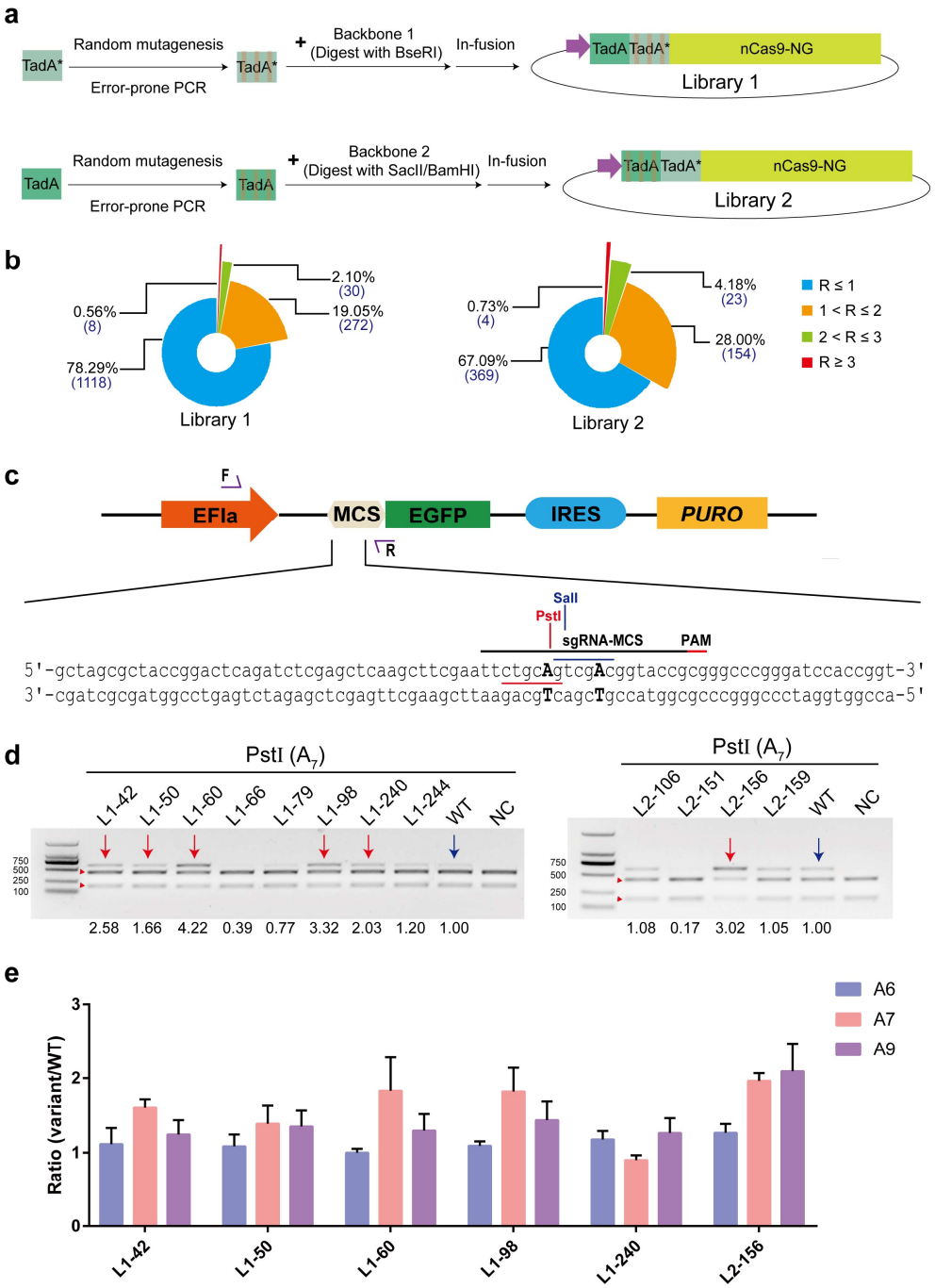

Fig. 2 Evolution of NG-ABEmax variants with improved A•T to G•C base editing activity.

a, Scheme of libraries generation design. The library 1 contain TadA* mutations and the library 2 contain TadA mutations. Red lines represent the point mutations. **b,** Summary of the library 1 and library 2 (A•T to G•C base editing efficiencies at A12). R represents the ratio of editing efficiency of mutants to NG-ABEmax. **c,** Schematic for assessing A•T to G•C base editing efficiencies of NG-ABEmax variants using the HEK293-PME cell line. Restriction sites are highlighted in red and blue. **d,** Agarose gel electrophoresis results of testing editing efficiency of NG-ABEmax variants with PstI. Cleaved bands from PstI are labeled with red triangle. The amplicon is 606-bp. The variants with high-activities are highlighted with red arrows. WT represents NG-ABEmax and highlighted with blue arrows. **e,** Boosted editing efficiencies of selected variants via *EGFP*-based reporter system**.** Error bars indicate mean ± s.d. of three technical replicates.

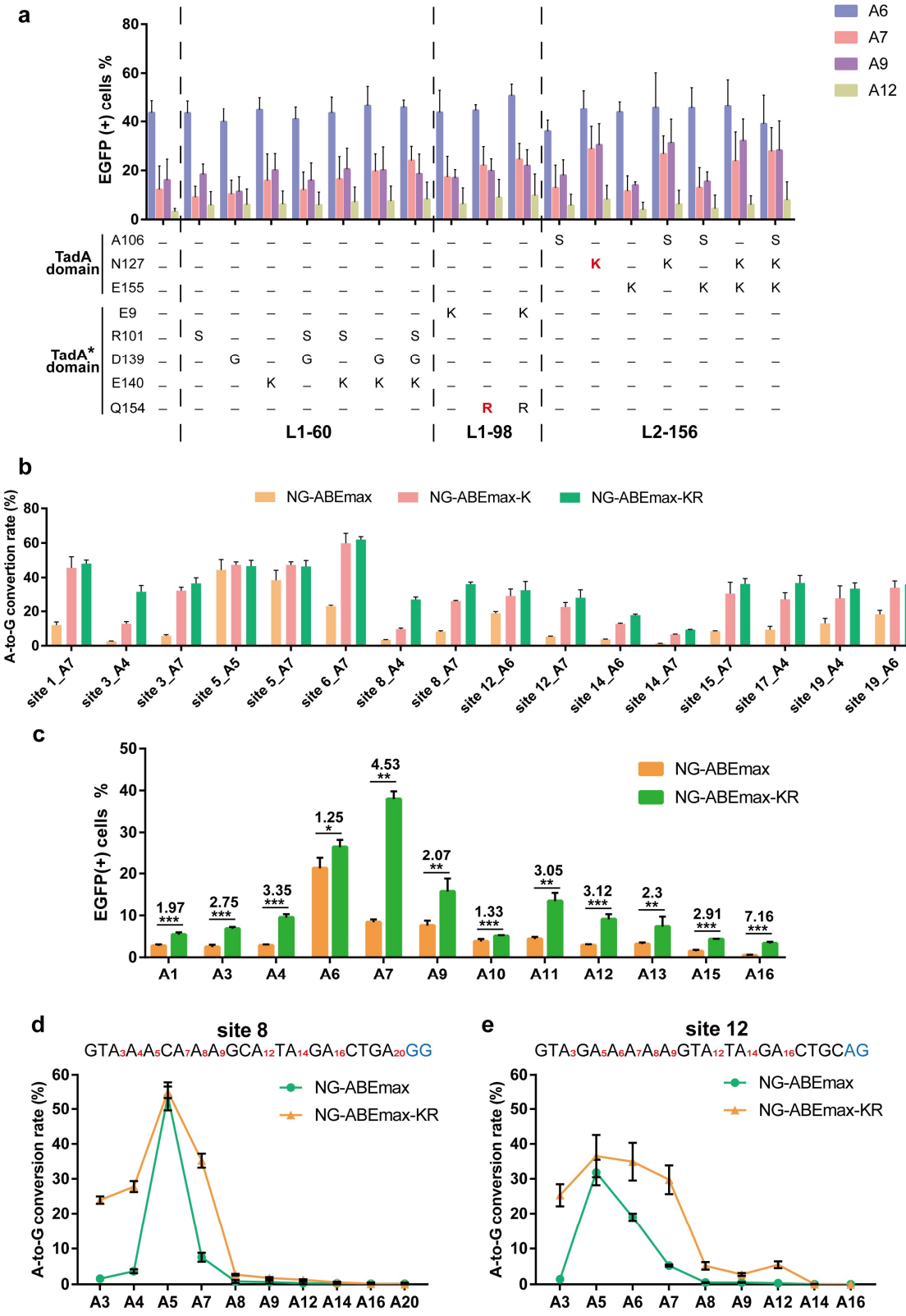

Fig. 3 Engineering of the NG-ABEmax variants.

a, Mapping the key residues for L1-60, L1-98 and L2-156 using *EGFP*-based reporter system. Editing efficiencies were quantified by flow cytometry. **b,** Boosted editing efficiencies of NG-ABEmax-KR at endogenous genomic sites. **c,** Summary of boosted editing efficiencies of NG-ABEmax-KR at different A base at the EGFP sites. Error bars indicate mean ± s.d. of three technical replicates. **d, e,** Increased editing window of NG-ABEmax-KR in site 8 and site 10. Each A base was highlighted in red. Error bars indicate mean ± s.d. of three technical replicates.

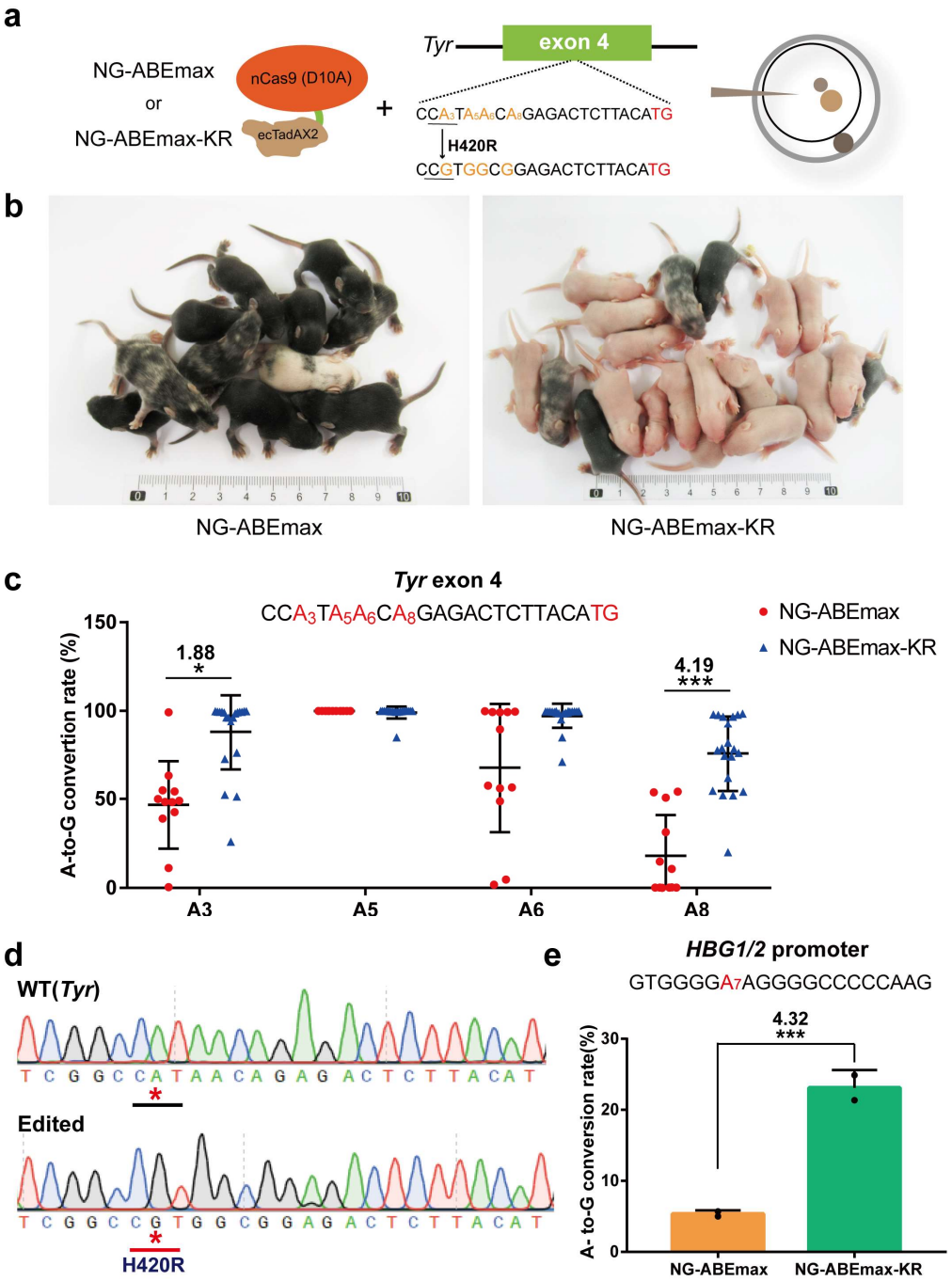

Fig. 4 Application of NG-ABEmax-KR for the generation of mice disease models and human gene therapy. **a,** Schematic of comparing editing activity of NG-ABEmax and NG-ABEmax-KR in mouse embryos via zygote intracytoplasmic injection. **b,** The newborn pups (days 10) produced by intracytoplasmic injection of NG-ABEmax or NG-ABEmax-KR mRNA and *Tyr* sgRNA The *Tyr* mutant mice (H420R) are in white and the wild-type are in black, respectively. **c,** Statistical analysis of on-target A-to-G base conversions induced by NG-ABEmax (n = 11), NG-ABEmaxKR (n = 20) in all pups. Data are mean ± s.d for the indicated numbers of mice. Each A base was highlighted in red. *P < 0.05, ***P < 0.001 by Student's unpaired two-sided t-test **d,** Sanger sequence chromatograms confirmed the editing events. The desired mutation was highlighted with red star. **e,** Boosted editing efficiency (A7) of NG-ABEmax-KR at *HBG1/2*.

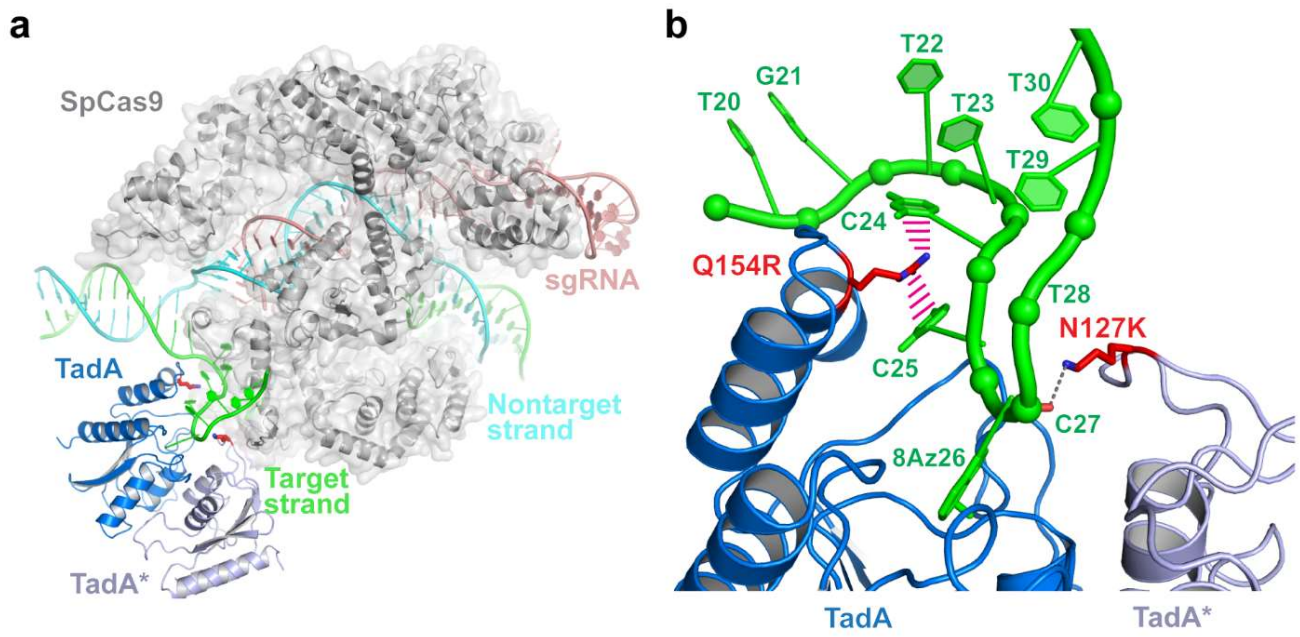

627

628 **Fig. 5 Molecular basis of enhanced editing efficiency of NG-ABEmax-KR.**

629 **a,** Overall structural model of NG-ABEmax-KR showing SpCas9 (gray), target-strand DNA (TS, green),
630 nontarget-strand DNA (NTS, cyan), single-target RNA (sgRNA, red), TadA (blue) and TadA* (light blue). The side
631 chains of N127K of TadA* and Q154R of TadA are shown as red sticks. **b,** Modelled Interactions between key residues
632 of NG-ABEmax-KR with TS DNA, colored as in (**a**).

Figures

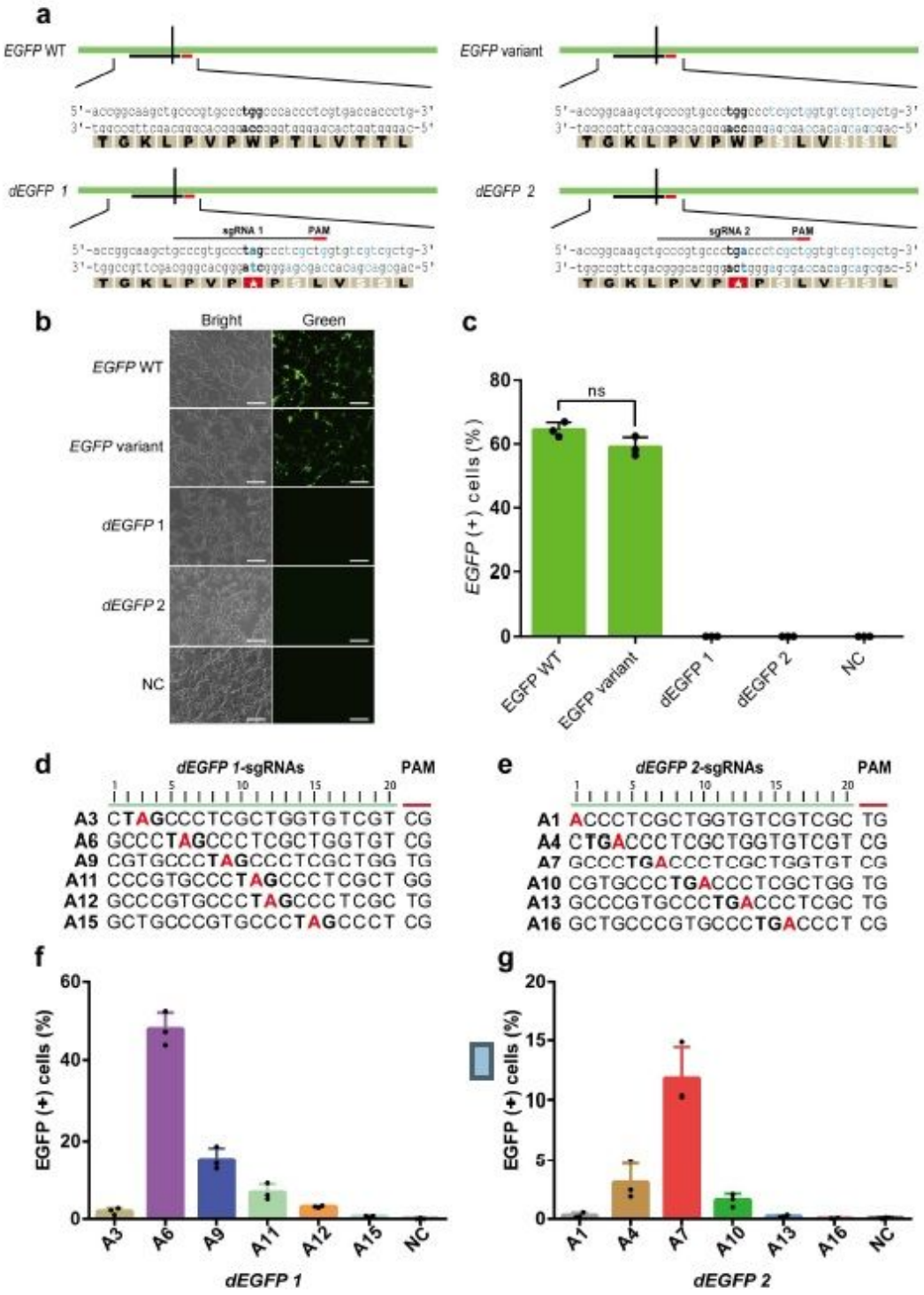

Figure 1

Design of the stop-codon reversion-based screening system. a, Different EGFP variants. Single nucleotide conversions are indicated by blue and residue substitutions are indicated by white. The stop codon was highlighted with red pentagram. b, c, Fluorescence image(b) and editing efficiencies(c) of HEK-293 cells

co-transfect with EGFP WT, variant, dEGFP 1 and dEGFP 2, respectively. EGFP variant maintains the expression, while dEGFP 1 and dEGFP 2 abolishes the expression. (c). EGFP positive cells were quantified by flow cytometry. Scale bar, 10 μm. Data are mean ± s.d. of three technical replicates. d, e, The sequence of different sgRNAs (5-'NG-3' PAM) which were suitable for dEGFP 1 and dEGFP 2, respectively. The stop codon and target A base have been highlighted in bold and red. f, g, Editing efficiencies of A to G mutations at different positions of dEGFP 1 and dEGFP 2. Error bars indicate mean ± s.d. of three technical replicates.

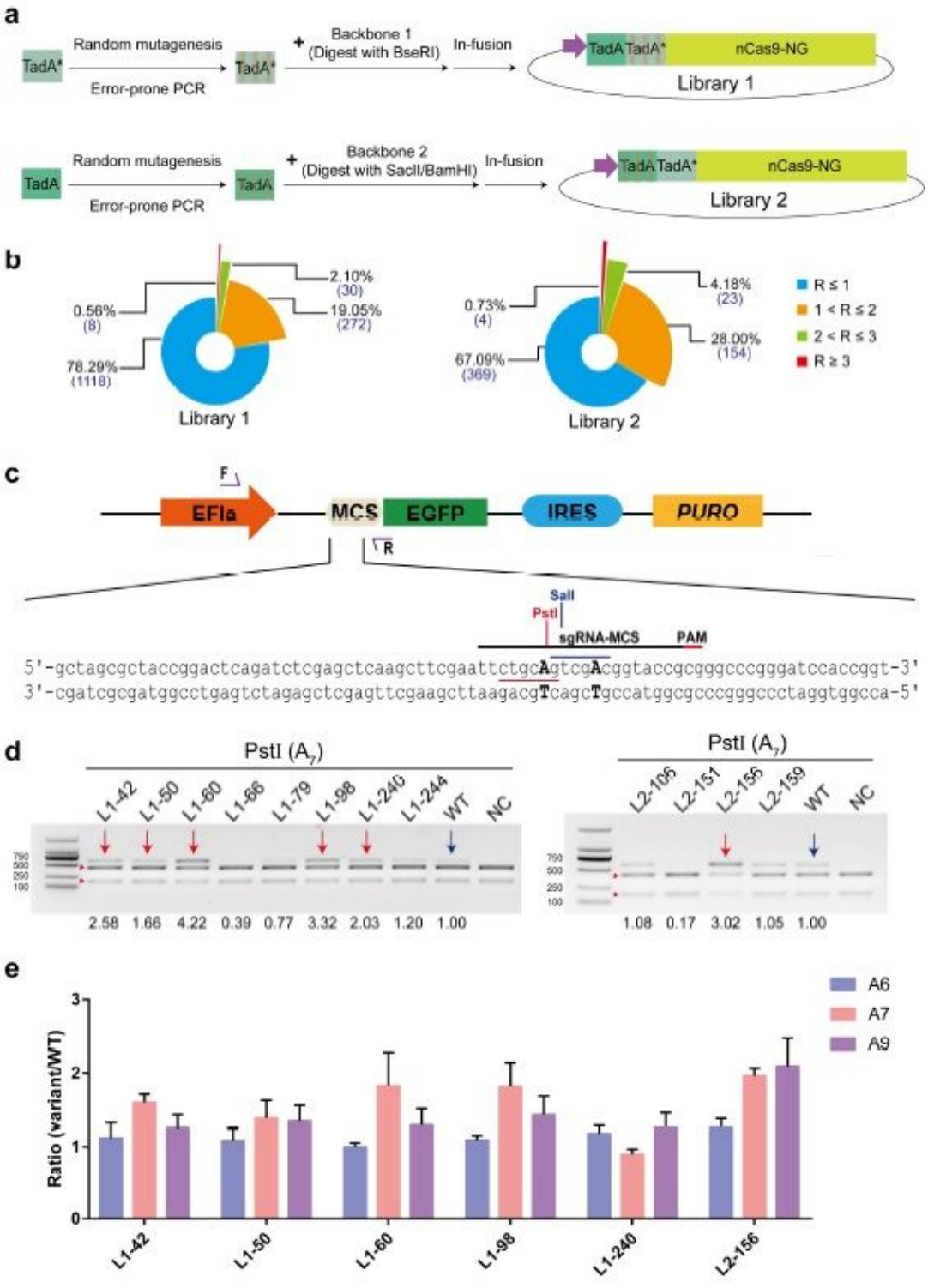

Figure 2

Evolution of NG-ABEmax variants with improved A•T to G•C base editing activity. a, Scheme of libraries generation design. The library 1 contain TadA* mutations and the library 2 contain TadA mutations. Red lines represent the point mutations. b, Summary of the library 1 and library 2 (A•T to G•C base editing efficiencies at A12). R represents the ratio of editing efficiency of mutants to NG-ABEmax. c, Schematic for assessing A•T to G•C base editing efficiencies of NG-ABEmax variants using the HEK293-PME cell line. Restriction sites are highlighted in red and blue. d, Agarose gel electrophoresis results of testing editing efficiency of NG-ABEmax variants with PstI. Cleaved bands from PstI are labeled with red triangle. The amplicon is 606-bp. The variants with high-activities are highlighted with red arrows. WT represents NG-ABEmax and highlighted with blue arrows. e, Boosted editing efficiencies of selected variants via EGFP-based reporter system. Error bars indicate mean ± s.d. of three technical replicates.

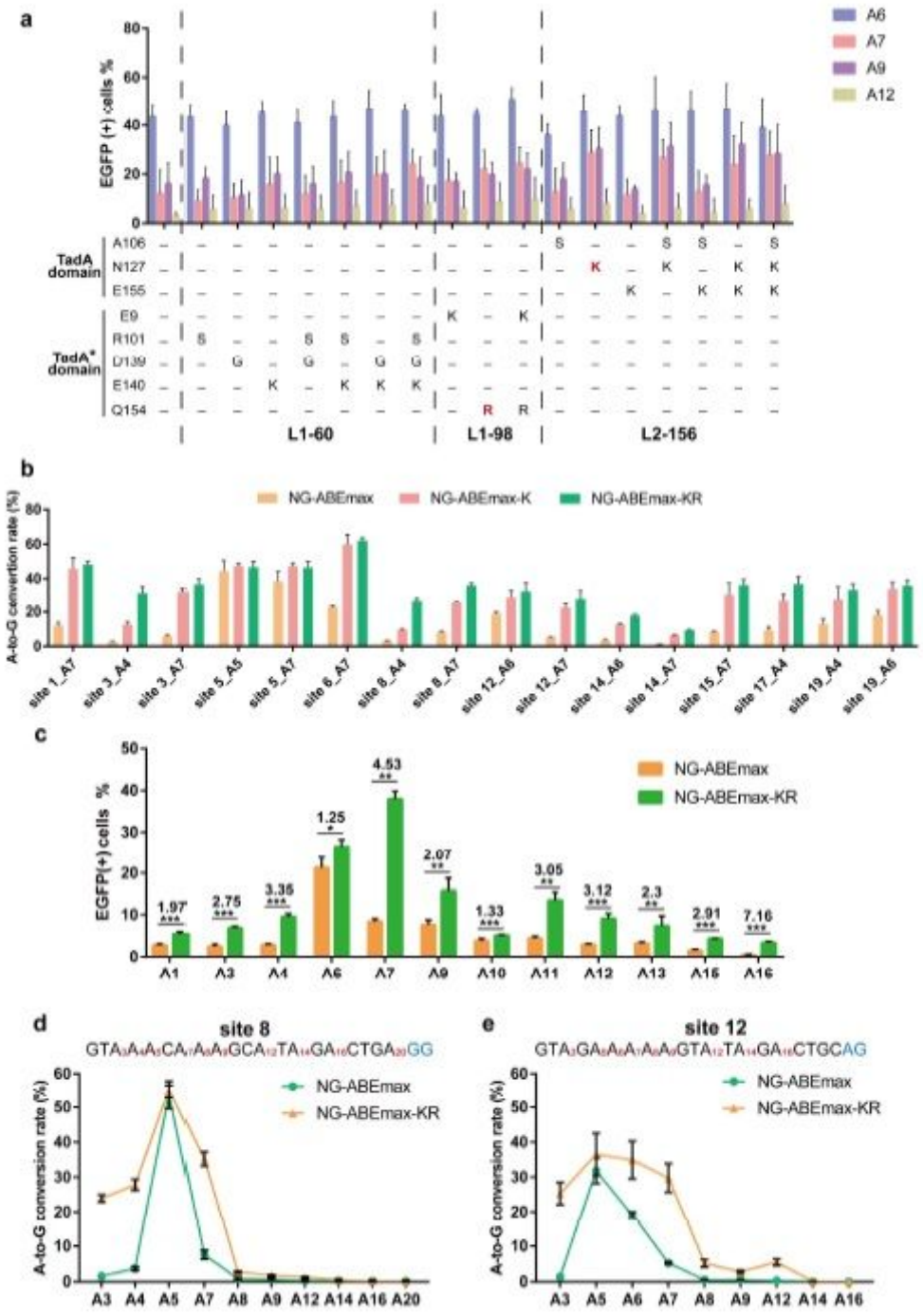

Figure 3

ngineering of the NG-ABEmax variants. a, Mapping the key residues for L1-60, L1-98 and L2-156 using EGFP-based reporter system. Editing efficiencies were quantified by flow cytometry. b, Boosted editing efficiencies of NG-ABEmax-KR at endogenous genomic sites. c, Summary of boosted editing efficiencies of NG-ABEmax-KR at different A base at the EGFP sites. Error bars indicate mean ± s.d. of three technical replicates. d, e, Increased editing window of NG-ABEmax-KR in site 8 and site 10. Each A base was highlighted in red. Error bars indicate mean ± s.d. of three technical replicates.

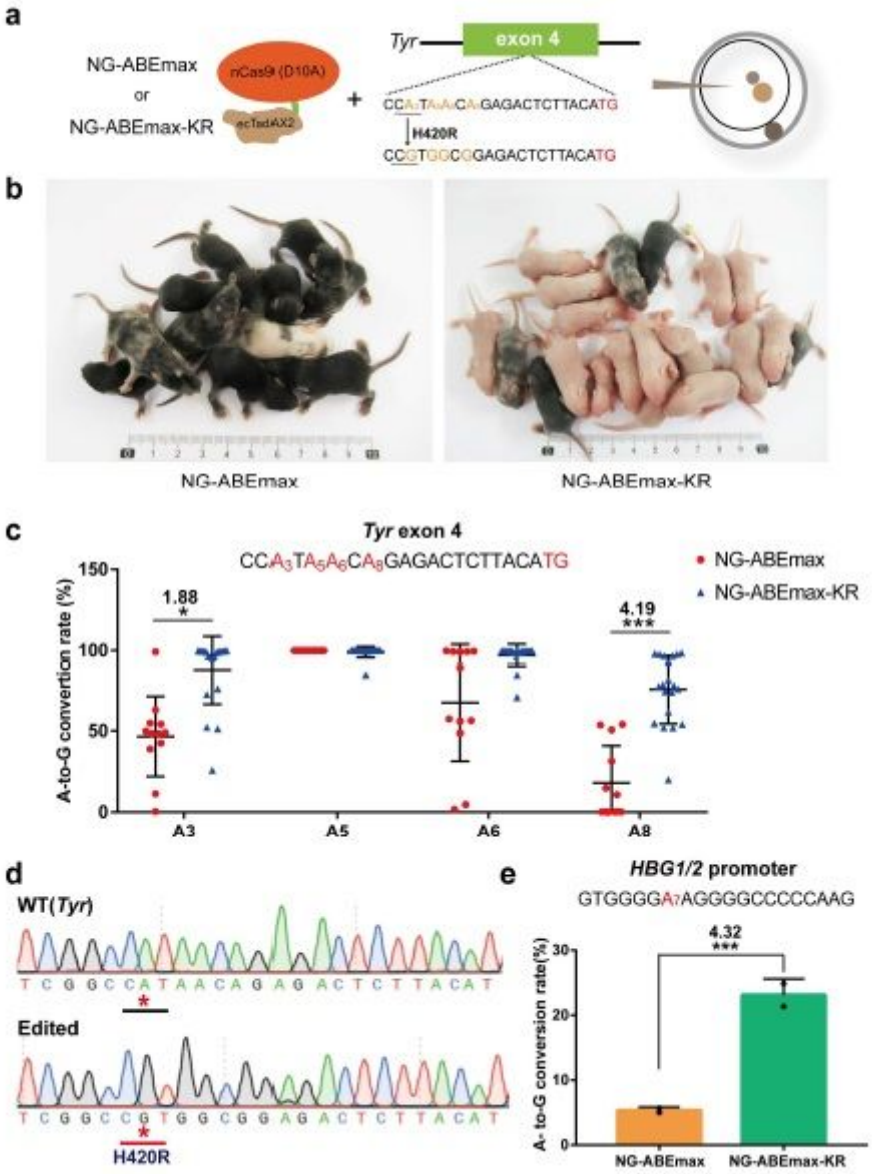

Figure 4

Application of NG-ABEmax-KR for the generation of mice disease models and human gene therapy. a, Schematic of comparing editing activity of NG-ABEmax and NG-ABEmax-KR in mouse embryos via zygote intracytoplasmic injection. b, The newborn pups (days 10) produced by intracytoplasmic injection of NG-ABEmax or NG-ABEmax-KR mRNA and Tyr sgRNA The Tyr mutant mice (H420R) are in white and the wild-type are in black, respectively. c, Statistical analysis of on-target A-to-G base conversions induced by NG-ABEmax (n = 11), NG-ABEmaxKR (n = 20) in all pups. Data are mean ± s.d for the indicated numbers of mice. Each A base was highlighted in red. *P < 0.05, ***P < 0.001 by Student's unpaired two-sided t-test d, Sanger sequence chromatograms confirmed the editing events. The desired mutation was highlighted with red star. e, Boosted editing efficiency (A7) of NG-ABEmax-KR at HBG1/2.

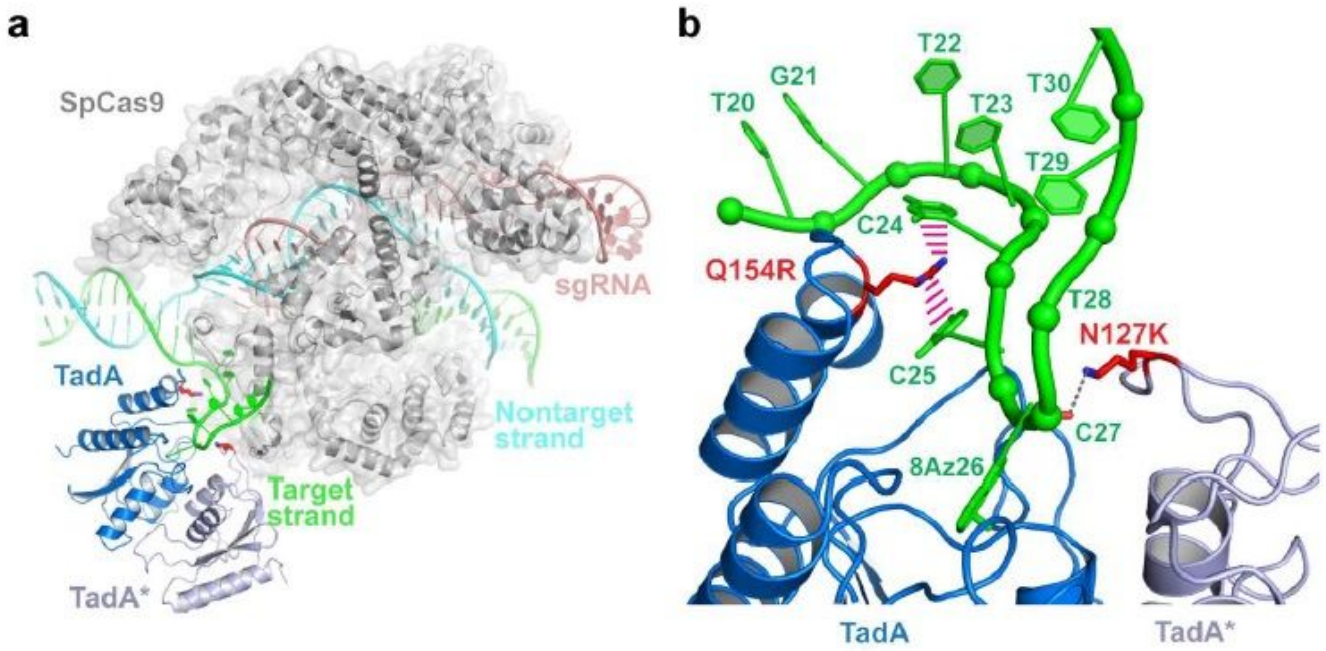

Figure 5

Molecular basis of enhanced editing efficiency of NG-ABEmax-KR. a, Overall structural model of NG-ABEmax-KR showing SpCas9 (gray), target-strand DNA (TS, green), nontarget-strand DNA (NTS, cyan), single-target RNA (sgRNA, red), TadA (blue) and TadA* (light blue). The side chains of N127K of TadA* and Q154R of TadA are shown as red sticks. b, Modelled Interactions between key residues of NG-ABEmax-KR with TS DNA, colored as in (a).

Supplementary Files

This is a list of supplementary files associated with this preprint. Click to download.

- Supplementarydata.pdf